Boundary Feedback Stabilization of Freeway Traffic Networks: ISS Control and Experiments

Liguo Zhang, Haoran Luan, Yusheng Lu, Christophe Prieur

Boundary Feedback Stabilization of Freeway Traffic Networks: ISS Control and Experiments

Liguo Zhang, Haoran Luan, Yusheng Lu, and Christophe Prieur

***Abstract*— Boundary feedback control of networks of freeway traffic is considered in this paper by means of Partial Differential Equations (PDEs) based techniques. The control and measurements are all located at the boundaries of each link. We have established the boundary control model for the system, a linear hyperbolic system of balance laws, which includes not only the traffic flow dynamics of the network described by combining the linearized Aw-Rascle-Zhang (ARZ) traffic flow model of each link, but also the integrated on-ramping metering and variable speed limit control modeled as the boundary condition. As the traffic demand of the network is fluctuated, the boundary Input-to-State Stability (ISS) controller is designed to suppress the disturbance and regulate the traffic flow into the boundedness regions of the desired states. Based on a novel Lyapunov function, some sufficient conditions in terms of the matrix inequalities are derived for the ISS boundary stabilization in the L^2 norm. The numerical simulation is given to illustrate the effectiveness of the developed boundary feedback control. Moreover, an interesting traffic experiment is carried out by using the traffic simulation software, AIMSUN, and some specific traffic data are collected and analyzed to verify the feasibility and effectiveness of the boundary control.**

***Index Terms*— Freeway traffic networks, traffic flow model, boundary feedback control, input-to-state stability, AIMSUN.**

I. Introduction

INSTABILITIES of traffic flow resulting in traffic waves, also terms stop-and-go waves, are caused by the delay of drivers in adapting their speed to the present traffic conditions. Therefore, for freeway traffic, the most fundamental control objective is to maintain the traffic variables, speed and density of the network, at the steady-state values and suppress the tendency to oscillations as much as possible. Adopting boundary feedback control is particularly natural and necessary for the freeway traffic, since the available control measures including on-ramp metering applied with the traffic lights at the on-ramps and the variable speed limits displayed on the Variable Message Signs (VMSs), are usually located at the boundaries between the freeway links.

The management and control of the freeway traffic has been considered for a long time as reported in the survey [15] which involves a comprehensive bibliography. Starting from proportional and heuristic feedback control approaches, variously advanced control methods are progressively investigated. Among other relevant reference, we may mention for instance:

- MPC for the coordination of ramp metering and variable speed limits has been especially developed and studied in [10] on the basis of finite-dimensional discrete linear approximations of the macroscopic traffic flow model, METANET, in [7].
- Exponential stabilization of the network of freeway traffic has also been formulated and analyzed in [11], on the basis of the discrete METANET model, to regulate speed and density converging to the steady-states.
- Optimal on-ramp metering technique has been developed in [8] on the basis of Cell Transmission Models (CTMs) of [5], a Godunov discrete scheme for the first-order PDE equation formulated as the classical LWR traffic flow model, in [13], [16].

During the recent years, PDEs-based techniques for traffic flow control has attracted wild attention. One of the advantages is that the control design is derived directly from the continuous LWR or second-order ARZ models, without any model approximation, linearization and discretisation, meanwhile remaining the main characteristics of traffic flows.

Backstepping and Lyapunov's method are two methods to design boundary feedback control for PDEs-based traffic flow models. In [21], according to the transmission direction of characteristic velocities, the linearized ARZ model is divided firstly into free-flow and congestion regimes. Then boundary feedback control is developed in [18] via backstepping method to reduce the stop-and-go oscillations of the congestion traffic regime. While, a Proportional-Integral (PI) boundary controller is considered in [24] for the linearized ARZ model, and further in [25] for the general quasi-linear case to stabilize the outside uncertain traffic demand, respectively, by means of the Lyapunov function method.

On the other hand, some more interesting traffic phenomena could been considered based on the PDEs-based traffic flow model. For example, a novel bilateral backstepping boundary

This work was partially supported by the National Natural Science Foundation of China (NSFC, grant No. 61873007), the Beijing Natural Science Foundation (grant No. 1182001), and the MIAI@Grenoble Alpes (ANR-19-P3IA-0003) *(Corresponding author: Liguo Zhang.)*

L. Zhang is with the Key Laboratory of Computational Intelligence and Intelligent Systems, Faculty of Information Technology, Beijing University of Technology, 100124, Beijing, China (e-mail: zhangliguo@bjut.edu.cn).

H. Luan is with the Faculty of Information Technology, Beijing University of Technology, 100124, Beijing, China (e-mail: luanhaoran@emails.bjut.edu.cn).

Y. Lu is with the Faculty of Information Technology, Beijing University of Technology, 100124, Beijing, China (e-mail: luyusheng2017@emails.bjut.edu.cn).

C. Prieur is with CNRS, Gipsa-lab, Univ. Grenoble Alpes, F-38000, Grenoble, France (e-mail: christophe.prieur@gipsa-lab.fr).

Color versions of one or more of the figures in this paper are available online at http://ieeexplore.ieee.org.

control is developed in [19] to stabilize a moving shockwave in a freeway segment on the basis of LWR model of congestion traffic. For traffic consisting of both Adaptive Cruise Control (ACC) equipped and manual vehicles, based on ARZ model, [4] presents a control design for stabilization of congestion traffic, in which the control input is the the time-gap setting of ACC-equipped vehicles. A Markov jumped hyperbolic system and the stochastic stability for ARZ model are formulated in [22] to model the stochastic traffic flow with uncertain characteristic velocities.

In this paper, we consider the boundary feedback control for the freeway network of traffic flows by using the linearized ARZ models. A hyperbolic system of balance laws is built for the control, which includes not only speed-density equations of links, but the integrated on-ramping metering and variable speed limit control as boundary conditions. Different feedback control strategies are designed for the different traffic regimes.

Then the problem of ISS control for the freeway traffic flow is formulated in the L^2 norm to deal with the disturbances of the network, such as the flux fluctuation suffering from the uncertain traffic demand of driving-in vehicles from the upstream mainline or driving-out from off-ramps. The sufficient condition in terms of a set of matrix inequalities is derived to guarantee the ISS of the freeway network by means of the Lyapunov-based techniques. Finally, the effectiveness of the developed boundary feedback control is illustrated with a numerical simulation and a particular traffic experiment, respectively, in which the traffic simulation software, AIMSUN is used to reproduce a portion of freeway traffic at the Fourth-Ring road of Beijing, China.

The paper is organized as follows. In Section II, a hyperbolic system of balance laws is formulated to model the network of freeway traffic. The sufficient condition for the ISS of networks of traffic flow is presented in Section III. In Section IV, a numerical simulation and a experiment are provided to evaluate the effectiveness of the boundary feedback control. Section V concludes the paper and introduces the directions for future research.

Notation. $\mathbb{R}$, $\mathbb{R}^n$, and $\mathbb{R}^{n\times n}$ denote the set of real numbers, n-order real vectors and n-order real matrices. For a matrix A, $A^\top$ denotes the transpose matrix, $|A|$ denotes the matrix of absolute values of A. $A < (\leq)\ 0$ denotes A is a negative definite (semi-definite) matrix. $\text{diag}\{x_1,\ldots,x_n\}$ is the block diagonal matrix formed with $x_i \in \mathbb{R}$, $i = 1,\ldots,n$. E_n is the identity matrix of the order n. Given a function $g \in L^2((0,L);\mathbb{R}^n)$, we mean that $\|g\|_{L^2} = \sqrt{\int_0^L g^\top(x)g(x)dx} < \infty$.

II. Freeway Traffic Modeling and Boundary Control

A local inhomogeneous network of the freeway traffic may be represented by a directed graph which consists of a set of links and nodes, as shown in Fig. 1. A freeway stretch between two successive on-ramps and without the inside merging zones is defined as the link. Inside each link, we suppose that there are homogeneous properties of roads such as the number of lanes, the free speed, the maximal density, etc. For each link

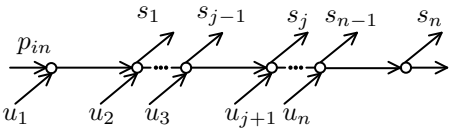

Fig. 1. A local inhomogeneous network of freeway traffic (the arrows represent flow of vehicles).

j, $j = 1,\ldots,N$, let L_j be the length, and I_j the number of lanes.

To facilitate the modeling and control of the freeway traffic network, for every link j, $j = 1,\ldots,N$, we assume that there is only one on-ramp located at the upstream boundary of the link, and only one off-ramp located at the downstream boundary. For the node, which connects the upstream link j and the downstream link $j+1$, we use u_{j+1} to denote the driving-in flux rate of vehicles from the on-ramp into the link $j+1$, and s_j the driving-out flux of vehicles from the off-ramp of the link j.

The traffic demand p_{in} is the flux rate of vehicles that drive into the freeway network through the beginning node.

A. Links

1) ARZ Traffic Flow Model: The macroscopic traffic flow dynamics on the line of the freeway link j are described by the quasi-linear hyperbolic systems of balance laws, the so-called Aw-Rascle-Zhang model of [1] as

$$\begin{cases} \partial_t \rho_j + \partial_x (\rho_j v_j) = 0, \\ \partial_t (v_j + p(\rho_j)) + v_j \partial_x (v_j + p(\rho_j)) = \frac{V(\rho_j) - v_j}{\tau}, \end{cases} \tag{1}$$

where $x \in [0, L_j)$, $t \in [0,\infty)$, $\rho_j : [0,L_j)\times[0,\infty) \to \mathbb{R}$ is the vehicle density, $v_j : [0,L_j)\times[0,\infty) \to \mathbb{R}$ is the average speed, and $p(\rho_j)$ is an increasing pressure function. τ is the relaxation term related to the driving behavior. $V(\rho_j)$ is the speed-density fundamental diagram typically in the form of Greenshields [9] as

$$V(\rho_j) = v_f \left(1 - \left(\frac{\rho_j}{\rho_m}\right)^\gamma\right), \tag{2}$$

where v_f is the free speed, ρ_m is the maximal density, and $\gamma > 0$ is a constant.

In [20], the pressure function is defined as

$$p(\rho_j) = v_f - V(\rho_j). \tag{3}$$

Combined with the Greenshields fundamental diagram of (2), the pressure term is specifically given as

$$p(\rho_j) = \frac{v_f}{\rho_m^\gamma}\rho_j^\gamma = a\rho_j^\gamma, \tag{4}$$

with $a = \frac{v_f}{\rho_m^\gamma}$.

One of the main characteristics of the hyperbolic PDEs is the existence of the Riemann coordinate transformation. Let

$$\begin{aligned} \omega_j &= v_j + a\rho_j^\gamma, \\ z_j &= v_j, \end{aligned} \tag{5}$$

then the ARZ model (1) can be described under the Riemann coordinate as

$$\begin{cases} \partial_t \omega_j + z_j \partial_x \omega_j = \frac{v_f - \omega_j}{\tau}, \\ \partial_t z_j + [(1+\gamma) z_j - \gamma\omega_j]\partial_x z_j = \frac{v_f - \omega_j}{\tau}. \end{cases} \tag{6}$$

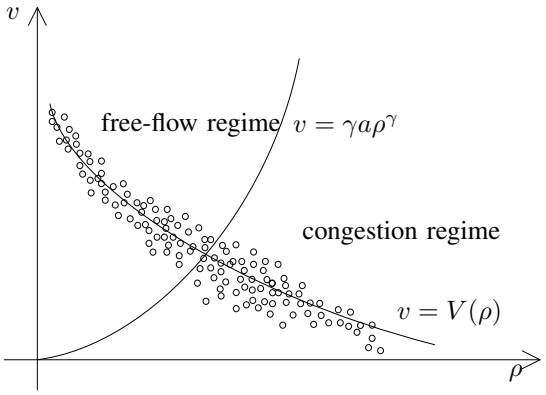

Fig. 2. Speed-density fundamental diagram with the free-flow regime and the congestion regime.

2) Linearization of ARZ Model: To regulate the traffic flow dynamics around the constant steady state $\left(\rho_j^*, v_j^*\right)$ of each link j, $j = 1, \ldots, N$, with $\omega_j^* = v_j^* + a\rho_j^{*\gamma}$, $z_j^* = v_j^*$, we firstly linearize the ARZ model (1) as following.

Define the deviations of the state ρ_j, v_j with respect to the state $\left(\rho_j^*, v_j^*\right)$ as

$$\begin{aligned} \tilde{\rho}_j &= \rho_j - \rho_j^*, \\ \tilde{v}_j &= v_j - v_j^*. \end{aligned} \tag{7}$$

Using the definitions $\tilde{\omega}_j = \omega_j - \omega_j^*$, and $\tilde{z}_j = z_j - z_j^*$, the linearized system $(\tilde{\omega}_j, \tilde{z}_j)$ around the desired state $\left(\omega_j^*, z_j^*\right)$, after removing the quasi-linear terms, is

$$\begin{cases} \partial_t \tilde{\omega}_j + z_j^* \partial_x \tilde{\omega}_j = \frac{v_f - \left(\tilde{\omega}_j + \omega_j^*\right)}{\tau}, \\ \partial_t \tilde{z}_j + \left[(1+\gamma) z_j^* - \gamma \omega_j^*\right] \partial_x \tilde{z}_j = \frac{v_f - \left(\tilde{\omega}_j + \omega_j^*\right)}{\tau}. \end{cases} \tag{8}$$

Denote the characteristic eigenvalues of the linearized system (8) are

$$\begin{aligned} \lambda_j^1 &= z_j^* = v_j^*, \\ \lambda_j^2 &= (1+\gamma) z_j^* - \gamma \omega_j^* = v_j^* - \gamma a \rho_j^{*\gamma}. \end{aligned} \tag{9}$$

We assume that the linearized system (8) is strictly hyperbolic, i.e. $\lambda_j^1 > 0$, and $\lambda_j^2 \neq 0$. Then according to the sign of the second eigenvalue λ_j^2, the speed-density relationship can be divided into two separated parts, named the free-flow regime and the congestion regime, respectively.

- Free-flow regime. In this case, $\lambda_j^2 > 0$, i.e. $v_j^* > \gamma a \rho_j^{*\gamma}$, the speed information of the linearized ARZ model of (8) is transmitted from the left boundary of the link $x = 0$ to the right boundary $x = L_j$. The characteristic velocity of the free-flow regime is located above the curve $v_j = \gamma a \rho_j^{\gamma}$, as shown in Fig. 2.
- Congestion regime. In this case, $\lambda_j^2 < 0$, i.e. $v_j^* < \gamma a \rho_j^{*\gamma}$, the speed information of the linearized ARZ model (8) is transmitted from the right boundary $x = L_j$ to the left $x = 0$. By contrast, the characteristic velocity of the congestion regime is located below the curve $v_j = \gamma a \rho_j^{\gamma}$. Since the first eigenvalue of $\lambda_j^1 > 0$ always holds, the hetero-directional propagations of traffic flow might lead to the shock waves of stop-and-go traffic.

Since the desired traffic state or the control object $\left(\rho_j^*, v_j^*\right)$ of each link might be selected arbitrarily, it may happen to satisfy the speed-density fundamental diagram of (2), i.e. $v_j^* = V\left(\rho_j^*\right)$. The linearized ARZ model can be expressed as

$$\begin{cases} \partial_t \tilde{\omega}_j + z_j^* \partial_x \tilde{\omega}_j = -\frac{\tilde{\omega}_j}{\tau}, \\ \partial_t \tilde{z}_j + \left[(1+\gamma) z_j^* - \gamma \omega_j^*\right] \partial_x \tilde{z}_j = -\frac{\tilde{\omega}_j}{\tau}. \end{cases} \tag{10}$$

As the desired state $\left(\rho_j^*, v_j^*\right)$, $j = 1, \ldots, N$ does not satisfy the speed-density fundamental diagram of the link j, i.e., $v_f - \omega_j^* \neq 0$, there exists a model drift from the set of steady states of the equation (8). In this case, the ISS of system (8) will be discussed later in Section III.

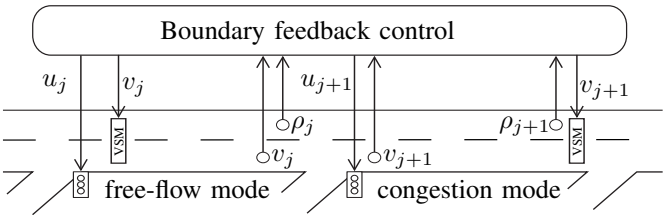

Fig. 3. Boundary control strategies for the freeway network of traffic flows.

3) Boundary Feedback Control: To regulate freeway traffic, we design the on-ramp metering controller $u_j(t)$ and two different variable speed limit controllers $v_j(0,t)$ or $v_j(L_j,t)$ at the link boundaries $x = 0$ or $x = L_j$, based on the regimes where the traffic lies in, as shown in Fig. 3.

On-ramp metering: No matter what kind of traffic regimes that the link j lies in, the first eigenvalue $\lambda_j^1 > 0$ still holds, so we should regulate the upstream on-ramp flow rate $u_j(t)$ based on the measurements collected from the downstream boundary $x = L_j$. Precisely, we define the boundary feedback control (ALINEA-typed on-ramp metering of [15]):

$$u_j(t) = u_j^* + k_j^{\rho}\left(\rho_j(L_j,t) - \rho_j^*\right), \tag{11}$$

where k_j^{ρ} is the feedback gain, and u_j^* is the normal regulation rate of the on-ramp.

Variable speed limit: To regulate the vehicle speed, two different control mechanisms of the variable speed limit are considered based on the traffic regime of the link j.

As the traffic of link j lies in the free-flow regime, the characteristic velocity of speed propagating is from upstream to downstream. It is natural to regulate the driving-in speed $v_j(0,t)$ based on the measurement $v_j(L_j,t)$ at the downstream boundary. Thus, the variable speed limit is:

$$v_j(0,t) = v_j^* + k_j^{v}\left(v_j(L_j,t) - v_j^*\right), \tag{12}$$

where k_j^{v} is the feedback gain for speed control.

On the other hand, as the link traffic lies in the congestion regime, the characteristic velocity of speed propagating is from downstream to upstream which is opposite to the case of the free-flow regime. Thus, we should regulate the downstream speed $v_j(L_j,t)$ based on the measurement $v_j(0,t)$ at the upstream boundary, i.e.,

$$v_j(L_j,t) = v_j^* + k_j^{v}\left(v_j(0,t) - v_j^*\right). \tag{13}$$

Then, in the following subsection, the developed on-ramp metering (11) and variable speed limit control (12), (13) for each link will be combined at the node to build the boundary condition of the network.

B. Node

The traffic dynamics of links are connected together at the nodes by means of the flux conservation laws of vehicles to model the freeway network of traffic flow.

1) Beginning Node: At the beginning node of the network, the traffic demand $p_{in}(t)$ of the mainline and $u_1(t)$ of the on-ramp are driving into the first link together based on the flux conservation law as follows:

$$p_{in}(t)+u_1(t)=\rho_1(0,t)\,v_1(0,t)\,I_1, \tag{14}$$

where $p_{in}(t)=p_{in}^*+\tilde{p}_{in}(t)$, p_{in}^* is the normal traffic demand, and $\tilde{p}_{in}(t)$ stands for the time-varying traffic fluctuation. Let u_1^* be the normal flux of the on-ramp, at the desired state, we have

$$p_{in}^*+u_1^*=\rho_1^* v_1^* I_1. \tag{15}$$

As the traffic of the first link lies in the free-flow regime, by combining the boundary feedback controller (11), (12) with conditions (14), (15) and assume $\gamma=1$, we have the boundary condition that

$$\begin{bmatrix}\tilde{\rho}_1(0,t)\\ \tilde{v}_1(0,t)\end{bmatrix}=\begin{bmatrix}\frac{k_1^\rho}{I_1 v_1^*} & -\frac{\rho_1^* k_1^v}{v_1^*}\\ 0 & k_1^v\end{bmatrix}\begin{bmatrix}\tilde{\rho}_1(L_1,t)\\ \tilde{v}_1(L_1,t)\end{bmatrix}+\begin{bmatrix}\frac{\tilde{p}_{in}}{I_1 v_1^*}\\ 0\end{bmatrix}.$$

For the $(\tilde{\omega}_j,\tilde{z}_j)$-system, we have

$$\begin{bmatrix}\tilde{\omega}_1(0,t)\\ \tilde{z}_1(0,t)\end{bmatrix}=G_f\begin{bmatrix}\tilde{\omega}_1(L_1,t)\\ \tilde{z}_1(L_1,t)\end{bmatrix}+\begin{bmatrix}\frac{a\tilde{p}_{in}}{I_1 v_1^*}\\ 0\end{bmatrix}, \tag{16}$$

where

$$G_f=\begin{bmatrix}\frac{k_1^\rho}{I_1 v_1^*} & k_1^v-\frac{a\rho_1^* k_1^v}{v_1^*}-\frac{k_1^\rho}{I_1 v_1^*}\\ 0 & k_1^v\end{bmatrix}. \tag{17}$$

Similarly, as the traffic of the first link lies in the congestion regime, by combining (11), (13) with (14), (15), we have

$$\begin{bmatrix}\tilde{\rho}_1(0,t)\\ \tilde{v}_1(L_1,t)\end{bmatrix}=\begin{bmatrix}\frac{k_1^\rho}{I_1 v_1^*} & -\frac{\rho_1^*}{v_1^*}\\ 0 & k_1^v\end{bmatrix}\begin{bmatrix}\tilde{\rho}_1(L_1,t)\\ \tilde{v}_1(0,t)\end{bmatrix}+\begin{bmatrix}\frac{\tilde{p}_{in}}{I_1 v_1^*}\\ 0\end{bmatrix}.$$

The boundary condition for the $(\tilde{\omega}_j,\tilde{z}_j)$-system is

$$\begin{bmatrix}\tilde{\omega}_1(0,t)\\ \tilde{z}_1(L_1,t)\end{bmatrix}=G_c\begin{bmatrix}\tilde{\omega}_1(L_1,t)\\ \tilde{z}_1(0,t)\end{bmatrix}+\begin{bmatrix}\frac{a\tilde{p}_{in}}{I_1 v_1^*}\\ 0\end{bmatrix}, \tag{18}$$

where

$$G_c=\begin{bmatrix}\frac{k_1^\rho}{I_1 v_1^*} & 1-\frac{a\rho_1^*}{v_1^*}-\frac{k_1^\rho k_1^v}{I_1 v_1^*}\\ 0 & k_1^v\end{bmatrix}. \tag{19}$$

2) Internal Node: For the internal node, which connects the upstream link j and the next downstream link $j+1$, for $j=1,\ldots,N$, we have

$$\begin{aligned}\rho_{j+1}(0,t)\,v_{j+1}(0,t)\,I_{j+1}=\rho_j(L_j,t)\,v_j(L_j,t)\,I_j\\ -s_j(t)+u_{j+1}(t),\end{aligned} \tag{20}$$

where $s_j(t)$ is the flux rate of vehicles driving-out from the off-ramp of link j, satisfies $s_j(t)=s_j^*+\tilde{s}_j(t)$. The normal flux rate of the off-ramp is s_j^*, and $\tilde{s}_j(t)$ stands for the bounded fluctuation of the exit flow.

When the traffic of link j and link $j+1$ both lie in the desired state, we have

$$\rho_{j+1}^* v_{j+1}^* I_{j+1}=\rho_j^* v_j^* I_j-s_j^*+u_{j+1}^*. \tag{21}$$

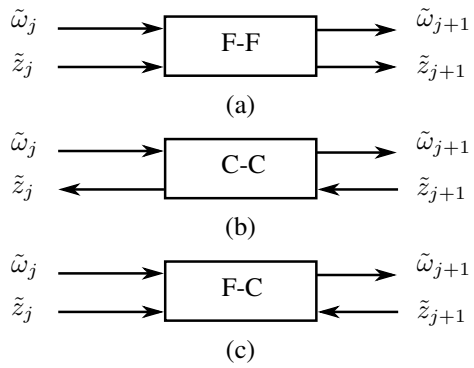

Fig. 4. Three different cases of the internal nodes: (a) F-F node; (b) C-C node; and (c) F-C node.

Since the link traffic might lie in the different regimes, the nodes could be divided into the following three cases:

- F-F node: The upstream link j and the downstream link $j+1$ both lie in the free-flow regime;
- C-C node: The upstream link j and the downstream link $j+1$ both lie in the congestion regime;
- F-C node: The upstream link j lies in the free-flow regime, while the downstream link $j+1$ in the congestion regime.

Three different cases of the internal nodes, through which the information of the traffic flow dynamics is transmitting, are shown in Fig. 4.

Remark 1: The node corresponding to a upstream link j lying in the congestion regime while the downstream $j+1$ lies in the free-flow, the so-called C-F case, is not considered here. Since the shock wave or congestion of traffic flow always propagates upward, as the downstream traffic lies in the free-flow regime, we could leave it out and only treat the upstream nodes as the C-C or F-C cases. Moreover, the rarefaction wave occurs as the traffic switches from congestion to free-flow. Some new assumptions should be added to set the initial values for the downstream free-flow regimes. ○

F-F Node: For the F-F node, combing the boundary feedback controllers (11), (12) for both links j and $j+1$, with the flux conservation law (20), we have the following boundary condition that

$$\begin{bmatrix}\tilde{\rho}_{j+1}(0,t)\\ \tilde{v}_{j+1}(0,t)\end{bmatrix}=G_{ff}^{\rho v}\begin{bmatrix}\tilde{\rho}_j(L_j,t)\\ \tilde{\rho}_{j+1}(L_{j+1},t)\\ \tilde{v}_j(L_j,t)\\ \tilde{v}_{j+1}(L_{j+1},t)\end{bmatrix}+\begin{bmatrix}\frac{\tilde{s}_j(t)}{I_{j+1}v_{j+1}^*}\\ 0\end{bmatrix},$$

where

$$G_{ff}^{\rho v}=\begin{bmatrix}\frac{I_j v_j^*}{I_{j+1}v_{j+1}^*} & \frac{k_{j+1}^\rho}{I_{j+1}v_{j+1}^*} & \frac{I_j\rho_j^*}{I_{j+1}v_{j+1}^*} & -\frac{\rho_{j+1}^* k_{j+1}^v}{v_{j+1}^*}\\ 0 & 0 & 0 & k_{j+1}^v\end{bmatrix}.$$

For the $(\tilde{\omega}_j,\tilde{z}_j)$-system, we have

$$\begin{bmatrix}\tilde{\omega}_{j+1}(0,t)\\ \tilde{z}_{j+1}(0,t)\end{bmatrix}=G_{ff}\begin{bmatrix}\tilde{\omega}_j(L_j,t)\\ \tilde{\omega}_{j+1}(L_{j+1},t)\\ \tilde{z}_j(L_j,t)\\ \tilde{z}_{j+1}(L_{j+1},t)\end{bmatrix}+\theta_{ff}(t), \tag{22}$$

where

$$G_{ff}=\begin{bmatrix} \frac{I_j v_j^*}{I_{j+1}v_{j+1}^*} & 0 \\ \frac{k_{j+1}^{\rho}}{I_{j+1}v_{j+1}^*} & 0 \\ \frac{aI_j\rho_j^*-I_j v_j^*}{I_{j+1}v_{j+1}^*} & 0 \\ k_{j+1}^{v}-\frac{a\rho_{j+1}^* k_{j+1}^{v}}{v_{j+1}^*}-\frac{k_{j+1}^{\rho}}{I_{j+1}v_{j+1}^*} & k_{j+1}^{v} \end{bmatrix}^{\top}, \tag{23}$$

$$\theta_{ff}(t)=\begin{bmatrix} \frac{a\tilde{s}_j(t)}{I_{j+1}v_{j+1}^*} & 0 \end{bmatrix}^{\top}.$$

C-C Node: For the C-C node, in this case, by combing the boundary controllers (11), (13) for both links j and $j+1$, with the flux conservation law (20), we have

$$\begin{bmatrix} \tilde{\rho}_{j+1}(0,t) \\ \tilde{v}_{j+1}(L_{j+1},t) \end{bmatrix}=G_{cc}^{\rho v}\begin{bmatrix} \tilde{\rho}_j(L_j,t) \\ \tilde{\rho}_{j+1}(L_{j+1},t) \\ \tilde{v}_j(0,t) \\ \tilde{v}_{j+1}(0,t) \end{bmatrix}+\begin{bmatrix} \frac{\tilde{s}_j(t)}{I_{j+1}v_{j+1}^*} \\ 0 \end{bmatrix}$$

where

$$G_{cc}^{\rho v}=\begin{bmatrix} \frac{I_j v_j^*}{I_{j+1}v_{j+1}^*} & \frac{k_{j+1}^{\rho}}{I_{j+1}v_{j+1}^*} & \frac{I_j\rho_j^* k_j^{v}}{I_{j+1}v_{j+1}^*} & -\frac{\rho_{j+1}^*}{v_{j+1}^*} \\ 0 & 0 & 0 & k_{j+1}^{v} \end{bmatrix}.$$

For the $(\tilde{\omega}_j,\tilde{z}_j)$-system

$$\begin{bmatrix} \tilde{\omega}_{j+1}(0,t) \\ \tilde{z}_{j+1}(L_{j+1},t) \end{bmatrix}=G_{cc}\begin{bmatrix} \tilde{\omega}_j(L_j,t) \\ \tilde{\omega}_{j+1}(L_{j+1},t) \\ \tilde{z}_j(0,t) \\ \tilde{z}_{j+1}(0,t) \end{bmatrix}+\theta_{cc}(t), \tag{24}$$

where

$$G_{cc}=\begin{bmatrix} \frac{I_j v_j^*}{I_{j+1}v_{j+1}^*} & 0 \\ \frac{k_{j+1}^{\rho}}{I_{j+1}v_{j+1}^*} & 0 \\ \frac{aI_j\rho_j^* k_j^{v}-I_j v_j^* k_j^{v}}{I_{j+1}v_{j+1}^*} & 0 \\ 1-\frac{a\rho_{j+1}^*}{v_{j+1}^*}-\frac{k_{j+1}^{\rho}k_{j+1}^{v}}{I_{j+1}v_{j+1}^*} & k_{j+1}^{v} \end{bmatrix}^{\top}, \tag{25}$$

$$\theta_{cc}(t)=\begin{bmatrix} \frac{a\tilde{s}_j(t)}{I_{j+1}v_{j+1}^*} & 0 \end{bmatrix}^{\top}.$$

F-C Node: For the F-C node, in this case, the traffic of link j is regulated with the boundary controller (11), (12), while link $j+1$ is regulated with (11), (13), respectively. After combing with the flux conservation law (20), we have the following boundary condition

$$\begin{bmatrix} \tilde{\rho}_{j+1}(0,t) \\ \tilde{v}_{j+1}(L_{j+1},t) \end{bmatrix}=G_{fc}^{\rho v}\begin{bmatrix} \tilde{\rho}_j(L_j,t) \\ \tilde{\rho}_{j+1}(L_{j+1},t) \\ \tilde{v}_j(L_j,t) \\ \tilde{v}_{j+1}(0,t) \end{bmatrix}+\begin{bmatrix} \frac{\tilde{s}_j(t)}{I_{j+1}v_{j+1}^*} \\ 0 \end{bmatrix}$$

where

$$G_{fc}^{\rho v}=\begin{bmatrix} \frac{I_j v_j^*}{I_{j+1}v_{j+1}^*} & \frac{k_{j+1}^{\rho}}{I_{j+1}v_{j+1}^*} & \frac{I_j\rho_j^*}{I_{j+1}v_{j+1}^*} & -\frac{\rho_{j+1}^*}{v_{j+1}^*} \\ 0 & 0 & 0 & k_{j+1}^{v} \end{bmatrix}.$$

Similarly, for the $(\tilde{\omega}_j,\tilde{z}_j)$-system, we have

$$\begin{bmatrix} \tilde{\omega}_{j+1}(0,t) \\ \tilde{z}_{j+1}(L_{j+1},t) \end{bmatrix}=G_{fc}\begin{bmatrix} \tilde{\omega}_j(L_j,t) \\ \tilde{\omega}_{j+1}(L_{j+1},t) \\ \tilde{z}_j(L_j,t) \\ \tilde{z}_{j+1}(0,t) \end{bmatrix}+\theta_{fc}(t), \tag{26}$$

where

$$G_{fc}=\begin{bmatrix} \frac{I_j v_j^*}{I_{j+1}v_{j+1}^*} & 0 \\ \frac{k_{j+1}^{\rho}}{I_{j+1}v_{j+1}^*} & 0 \\ \frac{aI_j\rho_j^*-I_j v_j^*}{I_{j+1}v_{j+1}^*} & 0 \\ 1-\frac{a\rho_{j+1}^*}{v_{j+1}^*}-\frac{k_{j+1}^{\rho}k_{j+1}^{v}}{I_{j+1}v_{j+1}^*} & k_{j+1}^{v} \end{bmatrix}^{\top}, \tag{27}$$

$$\theta_{fc}(t)=\begin{bmatrix} \frac{a\tilde{s}_j(t)}{I_{j+1}v_{j+1}^*} & 0 \end{bmatrix}^{\top}.$$

C. Network

In this subsection, we develop a linear hyperbolic system to model the network of freeway traffic. We firstly assume the upstream M links, $1\le M\le N$, lie in the free-flow regimes, while the downstream $N-M$ links lie in the congestion regimes. Furthermore, we assume the mainline traffic demand $p_{in}(t)$ could totally drive into the first link, and there is no constraint on the speed control $v_N(L_N,t)$ of the last link.

To simplify the notation, we firstly unify the spatial parameter $x\in[0,L_j]$, $j=1,\dots,N$ for the different length of links with a new parameter $y=\frac{x}{L_j}\in[0,1]$. Since $\gamma=1$, the new $(\tilde{\omega}_j,\tilde{z}_j)$-system is given as

$$\begin{cases} \partial_t\tilde{\omega}_j+\frac{z_j^*}{L_j}\partial_y\tilde{\omega}_j=\frac{v_f-(\tilde{\omega}_j+\omega_j^*)}{\tau}, \\ \partial_t\tilde{z}_j+\frac{2z_j^*-\omega_j^*}{L_j}\partial_y\tilde{z}_j=\frac{v_f-(\tilde{\omega}_j+\omega_j^*)}{\tau}, \end{cases} \tag{28}$$

where $y\in[0,1]$, $t\in[0,\infty)$, and $\tilde{\omega}_j$ stands for $\tilde{\omega}_j(y,t)$ and $\tilde{z}_j$ stands for $\tilde{z}_j(y,t)$.

Let us define a new vector $\xi:[0,1]\times[0,\infty)\to\mathbb{R}^{2N}$ as

$$\xi=\begin{bmatrix} \tilde{\omega}_1 & \dots & \tilde{\omega}_N & \tilde{z}_1 & \dots & \tilde{z}_N \end{bmatrix}^{\top}, \tag{29}$$

then the network model of freeway traffic flow of (28) can be described as a $2N$-order linear hyperbolic system of balance laws

$$\partial_t\xi+\Lambda\partial_y\xi=M\xi+b, \tag{30}$$

where

$$\Lambda=\mathrm{diag}\{\frac{z_1^*}{L_1},\dots,\frac{z_N^*}{L_N},\frac{2z_1^*-\omega_1^*}{L_1},\dots,\frac{2z_N^*-\omega_N^*}{L_N}\},$$

$$M=\begin{bmatrix} M_{11} & 0 \\ M_{12} & 0 \end{bmatrix},$$

with $M_{11}=M_{12}=\mathrm{diag}\{-\frac{1}{\tau},\dots,-\frac{1}{\tau}\}$, and the model drift

$$b=\begin{bmatrix} \frac{v_f-\omega_1^*}{\tau} & \dots & \frac{v_f-\omega_N^*}{\tau} & \frac{v_f-\omega_1^*}{\tau} & \dots & \frac{v_f-\omega_N^*}{\tau} \end{bmatrix}^{\top}.$$

The boundary condition of system (30) is constructed from the boundary feedback controller of links. As the network with the desired traffic states (ρ_j^*,v_j^*) of every link in the different regimes, we consider the boundary feedback controller as follows:

1) For the on-ramp metering, for all links, $j=1,\dots,N$, we have

$$u_j(t)=u_j^*+k_j^{\rho}\left(\rho_j(1,t)-\rho_j^*\right). \tag{31}$$

2) For the variable speed limit control of the upstream M links $j=1,\dots,M$, we have

$$v_j(0,t)=v_j^*+k_j^{v}\left(v_j(1,t)-v_j^*\right). \tag{32}$$

3) For the variable speed limit control of the downstream $N-M$ links $j=M+1,\ldots,N$, we have

$$v_j(1,t)=v_j^*+k_j^v\left(v_j(0,t)-v_j^*\right). \tag{33}$$

After combining the boundary feedback control (31)-(33) together, we get the input-output relationship (i.e., boundary condition) for the system (30)

$$\xi_{in}(t)=G\xi_{out}(t)+\theta(t), \tag{34}$$

where

$$\xi_{in}(t)=\left[\begin{array}{cccc}\tilde{\omega}_1(0,t) & \ldots & \tilde{\omega}_N(0,t) & \tilde{z}_1(0,t)\\ \tilde{z}_M(0,t) & \tilde{z}_{M+1}(1,t) & \ldots & \tilde{z}_N(1,t)\end{array}\right]^\top,$$

$$\xi_{out}(t)=\left[\begin{array}{cccc}\tilde{\omega}_1(1,t) & \ldots & \tilde{\omega}_N(1,t) & \tilde{z}_1(1,t)\\ \tilde{z}_M(1,t) & \tilde{z}_{M+1}(0,t) & \ldots & \tilde{z}_N(0,t)\end{array}\right]^\top,$$

$$\theta(t)=\left[\begin{array}{cccccc}\frac{a\tilde{p}_{in}(t)}{I_1v_1^*} & \frac{a\tilde{s}_1(t)}{I_2v_2^*} & \ldots & \frac{a\tilde{s}_{N-1}(t)}{I_Nv_N^*} & 0 & \ldots\ 0\end{array}\right]^\top.$$

The non-zero elements of the boundary condition matrix $G=[g_{i,j}]_{2N\times 2N}$ are given as

$$\begin{aligned}
&g_{i,i}=\tfrac{k_i^\rho}{I_iv_i^*},\ i=1,\ldots,N,\\
&g_{i,i-1}=\tfrac{I_{i-1}v_{i-1}^*}{I_iv_i^*},\ i=2,\ldots,N,\\
&g_{i,N+i}=k_i^v-\tfrac{a\rho_i^*k_i^v}{v_i^*}-\tfrac{k_i^\rho}{I_iv_i^*},\ i=1,\ldots,M,\\
&g_{i,N+i-1}=\tfrac{aI_{i-1}\rho_{i-1}^*-I_{i-1}v_{i-1}^*}{I_iv_i^*},\ i=2,\ldots,M+1,\\
&g_{i,N+i}=1-\tfrac{a\rho_i^*}{v_i^*}-\tfrac{k_i^\beta k_i^v}{I_iv_i^*},\ i=M+1,\ldots,N,\\
&g_{i,N+i-1}=\tfrac{aI_{i-1}\rho_{i-1}^*k_{i-1}^v-I_{i-1}v_{i-1}^*k_{i-1}^v}{I_iv_i^*},\ i=M+2,\ldots,N,\\
&g_{i,i}=k_i^v,\ i=N+1,\ldots,2N,
\end{aligned}$$

and the else elements are all zeros in G.

Remark 2: In the above network, we have assumed that $1\le M\le N$, then the traffic of the first link lies in the free-flow regime. If the whole freeway traffic is in the congestion regime, $M=0$, we can get the similar boundary condition as just re-establish the boundary condition of the first link with (19) and modify ξ_{in}, ξ_{out} and G accordingly. ∘

To summarize, we have established the control model for the network of freeway traffic, a linear hyperbolic system of balance laws, which includes not only the traffic flow dynamics of (30), but the integrated on-ramping metering and variable speed limit control modeled as the boundary condition of (34). The well-posedness of the Cauchy problem (30), (34) and the existence of the unique classical solutions follow from [3, Theorem B1].

The boundary stabilization for the network model of traffic flow (30), (34) will be discussed in the next section.

III. ISS Boundary Stabilization for Freeway Traffic Networks

The purpose of this section is to investigate the sufficient condition on the boundary feedback control (34), such that the solution of system (30) suppresses the disturbances $\theta(t)$ and the model drift b, no mater how many free-flow links M, and ultimately converges to a bounded region of the desired state (ρ_j^*,v_j^*), $j=1,\ldots,N$, as $t\to\infty$.

The definition of the ISS and the ISS-Lyapunov function for the system (30) are given as follows (see [14] for a recent survey of this notion for infinite-dimensional systems).

Definition 1: *The traffic flow network (30) and (34) is said to be ISS with respect to the model drift and disturbance $(b,\theta(t))$, if there exists a class $\mathcal{KL}$ function β_1 and a class $\mathcal{K}$ function β_2 such that, for any initial state $\xi_0\in L^2(0,1)$, the solution ξ of (30) and (34) satisfies, for all $t\ge 0$*

$$\|\xi(\cdot,t)\|_{L^2}\le\beta_1\left(\|\xi_0\|_{L^2},t\right)+\beta_2\left(\sup_{0\le\tau\le t}|(b,\theta(\tau))|\right). \tag{35}$$

Definition 2: *Let $V:L^2\left((0,1),\mathbb{R}^{2N}\right)\to\mathbb{R}$ be a continuously differentiable function such that, for all ξ in $L^2\left((0,1),\mathbb{R}^{2N}\right)$,*

$$\alpha_1\left(\|\xi\|_{L^2}\right)\le V(\xi)\le\alpha_2\left(\|\xi\|_{L^2}\right), \tag{36}$$

and such that, along all solutions to (30) and (34),

$$\dot{V}(t)\le-\nu V(t)+\alpha_3\left(|(b,\theta(t))|\right), \tag{37}$$

where α_1, α_2 are class $\mathcal{K}_\infty$ functions, α_3 is a class $\mathcal{K}$ function, and $\nu>0$ is a positive real number, the function V called an ISS-Lyapunov function for the system (30) and (34).

As the system (30), (34) admits an ISS-Lyapunov function V satisfying inequalities (36)-(37) of Definition 2, then the following inequality

$$\begin{aligned}
\|\xi(\cdot,t)\|_{L^2}\le&\alpha_1^{-1}\Big(e^{-\nu t}\alpha_2(\|\xi_0\|_{L^2})\\
&+\frac{1}{\nu}\sup_{0\le\tau\le t}\alpha_3(|(b,\theta(\tau))|)\Big)\\
\le&\alpha_1^{-1}\Big(2e^{-\nu t}\alpha_2(\|\xi_0\|_{L^2})\Big)\\
&+\alpha_1^{-1}\Big(\frac{2}{\nu}\sup_{0\le\tau\le t}\alpha_3(|(b,\theta(\tau))|)\Big),
\end{aligned} \tag{38}$$

holds, for all solutions to (30) and (34). Let $\beta_1(\cdot,t)=\alpha_1^{-1}(2e^{-\nu t}\alpha_2(\cdot))$, $\beta_2(\cdot)=\alpha_1^{-1}(2\nu^{-1}\alpha_3(\cdot))$, since Definition 1 we find the system (30), (34) is ISS in the L^2-norm. The ISS (or directly inequality (38)) gives an estimated bound of the influence of the model drift b and disturbance $\theta(t)$ on the traffic flow network (30) with the boundary feedback control (34).

The main result of this section is given as follows.

Theorem 1: *Consider the network of traffic flow (30), (34). If there exist constants $\mu\in\mathbb{R}$, $\kappa_1>0$, $\kappa_2>0$ and a diagonal positive definite matrix $P\in\mathbb{R}^{2N}$ such that the following inequalities hold, for all $y\in[0,1]$*

$$e^\mu G^\top|\Lambda|PG-|\Lambda|P+\frac{e^\mu\bar{\lambda}}{\kappa_1}E_{2N}\le 0, \tag{39}$$

$$M^\top\mathcal{P}(y)+\mathcal{P}(y)M-\mu|\Lambda|\mathcal{P}(y)+\lambda_{\max}\kappa_2E_{2N}<0, \tag{40}$$

where $\mathcal{P}(y)=Pdiag\{e^{\mu(1-y)}E_{N+M},e^{\mu y}E_{N-M}\}$, $\bar{\lambda}$, $\lambda_{\max}$ are the maximum eigenvalues of matrices $|\Lambda|PG$, $\mathcal{P}(y)$, for any y in $[0,1]$, respectively, then the system (30) is ISS with the boundary feedback condition (34).

Proof: We begin the proof by proposing an ISS-Lyapunov function candidate $V:L^2\left((0,1),\mathbb{R}^{2N}\right)\to\mathbb{R}$

defined by, for all ξ in $L^2\left((0,1),\mathbb{R}^{2N}\right)$,

$$V(t)=\int_0^1 \xi^\top \mathcal{P}(y)\xi dy, \tag{41}$$

with the specific $\mathcal{P}(y)=\text{diag}\{e^{\mu(1-y)}P_1, e^{\mu y}P_2\}$, the diagonal sub-matrices $P_1\in\mathbb{R}^{(N+M)\times(N+M)}$, and $P_2\in\mathbb{R}^{(N-M)\times(N-M)}$.

Considering the time derivative of V along the system (30), and using the integration by parts, we obtain

$$\begin{aligned}
\dot V(t)=&\int_0^1\left[\partial_t\xi^\top\mathcal{P}(y)\xi+\xi^\top\mathcal{P}(y)\partial_t\xi\right]dy\\
=&\int_0^1\Big[(-\Lambda\partial_y\xi+M\xi+b)^\top\mathcal{P}(y)\xi\\
&\qquad+\xi^\top\mathcal{P}(y)(-\Lambda\partial_y\xi+M\xi+b)\Big]dy\\
=&-\int_0^1\left[\partial_y\xi^\top\Lambda\mathcal{P}(y)\xi+\xi^\top\mathcal{P}(y)\Lambda\partial_y\xi\right]dy\\
&+\int_0^1\xi^\top\left[M^\top\mathcal{P}(y)+\mathcal{P}(y)M\right]\xi dy\\
&+\int_0^1\left[b^\top\mathcal{P}(y)\xi+\xi^\top\mathcal{P}(y)b\right]dy\\
=&-\xi^\top\Lambda\mathcal{P}(y)\xi\Big|_{y=0}^{y=1}\\
&+\int_0^1\xi^\top\left[M^\top\mathcal{P}(y)+\mathcal{P}(y)M-\mu|\Lambda|\mathcal{P}(y)\right]\xi dy\\
&+\int_0^1\left[b^\top\mathcal{P}(y)\xi+\xi^\top\mathcal{P}(y)b\right]dy\\
=&W_1+W_2+W_3,
\end{aligned}\tag{42}$$

with

$$W_1\triangleq\xi^\top(0,t)\Lambda\mathcal{P}(0)\xi(0,t)-\xi^\top(1,t)\Lambda\mathcal{P}(1)\xi(1,t), \tag{43}$$

$$W_2\triangleq\int_0^1\xi^\top[M^\top\mathcal{P}(y)+\mathcal{P}(y)M-\mu|\Lambda|\mathcal{P}(y)]\xi dy, \tag{44}$$

$$W_3\triangleq\int_0^1\left[b^\top\mathcal{P}(y)\xi+\xi^\top\mathcal{P}(y)b\right]dy. \tag{45}$$

Note that $\xi(0,t)$ includes the first $N+M$ elements of $\xi_{in}(t)$ and the left $N-M$ elements of $\xi_{out}(t)$, and denote $\xi(0,t)=[\xi_{in}^{N+M},\xi_{out}^{N-M}]$. Similarly, denote $\xi(1,t)=[\xi_{out}^{N+M},\xi_{in}^{N-M}]$. Substituting the boundary feedback condition (34) in W_1, and since both Λ, $\mathcal{P}(y)$ are diagonal matrices, we have

$$\begin{aligned}
W_1=&\xi^\top(0,t)\Lambda\mathcal{P}(0)\xi(0,t)-\xi^\top(1,t)\Lambda\mathcal{P}(1)\xi(1,t)\\
=&\xi^\top(0,t)\Lambda\text{diag}\{P_1e^{\mu},P_2\}\xi(0,t)\\
&-\xi^\top(1,t)\Lambda\text{diag}\{P_1,P_2e^{\mu}\}\xi(1,t)\\
=&[\xi_{in}^{N+M},\xi_{out}^{N-M}]^\top\Lambda\text{diag}\{P_1e^{\mu},P_2\}[\xi_{in}^{N+M},\xi_{out}^{N-M}]\\
&-[\xi_{out}^{N+M},\xi_{in}^{N-M}]^\top\Lambda\text{diag}\{P_1,P_2e^{\mu}\}[\xi_{out}^{N+M},\xi_{in}^{N-M}]\\
=&(\xi_{in}^{N+M})^\top\Lambda^{N+M}P_1e^{\mu}\xi_{in}^{N+M}\\
&+(\xi_{out}^{N-M})^\top\Lambda^{N-M}P_2\xi_{out}^{N-M}\\
&-(\xi_{out}^{N+M})^\top\Lambda^{N+M}P_1\xi_{out}^{N+M}\\
&-(\xi_{in}^{N-M})^\top\Lambda^{N-M}P_2e^{\mu}\xi_{in}^{N-M}\\
=&(\xi_{in}^{N+M})^\top|\Lambda|^{N+M}P_1e^{\mu}\xi_{in}^{N+M}\\
&-(\xi_{out}^{N+M})^\top|\Lambda|^{N+M}P_1\xi_{out}^{N+M}\\
&+(\xi_{in}^{N-M})^\top|\Lambda|^{N-M}P_2e^{\mu}\xi_{in}^{N-M}\\
&-(\xi_{out}^{N-M})^\top|\Lambda|^{N-M}P_2\xi_{out}^{N-M},
\end{aligned}\tag{46}$$

with the additional notation $\Lambda=\text{diag}\{\Lambda^{N+M},\Lambda^{N-M}\}=\text{diag}\{|\Lambda|^{N+M},-|\Lambda|^{N-M}\}$. Hence

$$\begin{aligned}
W_1=&e^{\mu}\xi_{in}^\top|\Lambda|P\xi_{in}-\xi_{out}^\top|\Lambda|P\xi_{out}\\
=&e^{\mu}(G\xi_{out}+\theta)^\top|\Lambda|P(G\xi_{out}+\theta)-\xi_{out}^\top|\Lambda|P\xi_{out}\\
=&\xi_{out}^\top(e^{\mu}G^\top|\Lambda|PG-|\Lambda|P)\xi_{out}+e^{\mu}\theta^\top|\Lambda|P\theta\\
&+e^{\mu}\left(\theta^\top|\Lambda|PG\xi_{out}+\xi_{out}^\top G^\top|\Lambda|P\theta\right).
\end{aligned}\tag{47}$$

Further using the Cauchy-Schwarz inequality to the last term of (47), it follows that

$$\begin{aligned}
W_1\leq&\xi_{out}^\top\left(e^{\mu}G^\top|\Lambda|PG-|\Lambda|P\right)\xi_{out}\\
&+e^{\mu}\bar\lambda\left(\kappa_1\theta^\top\theta+\frac{1}{\kappa_1}\xi_{out}^\top\xi_{out}\right)+e^{\mu}\theta^\top|\Lambda|P\theta\\
\leq&\xi_{out}^\top\left(e^{\mu}G^\top|\Lambda|PG-|\Lambda|P\right)\xi_{out}\\
&+\frac{e^{\mu}\bar\lambda}{\kappa_1}\xi_{out}^\top\xi_{out}+\ell\theta^\top\theta,
\end{aligned}\tag{48}$$

where $\bar\lambda$ is the maximum eigenvalue of $|\Lambda|PG$, for any parameter $\kappa_1>0$, and letting $\ell=e^{\mu}(\bar\lambda\kappa_1+|\Lambda|P)>0$.

On the other hand, for any constant $\kappa_2>0$ it holds

$$\begin{aligned}
W_3=&\int_0^1\left[b^\top\mathcal{P}(y)\xi+\xi^\top\mathcal{P}(y)b\right]dy\\
\leq&\lambda_{\max}\int_0^1\left[\kappa_2\xi^\top\xi+\frac{1}{\kappa_2}b^\top b\right]dy\\
=&\lambda_{\max}\kappa_2\int_0^1\xi^\top\xi dx+\frac{\lambda_{\max}}{\kappa_2}|b|^2.
\end{aligned}\tag{49}$$

Combining the above estimates (48), (49) with W_2, and using (39) and (40), we get the existence of a positive constant $\nu>0$, which depends on μ, P, and M, such that

$$\begin{aligned}
\dot V(t)=&W_1+W_2+W_3\\
\leq&\xi_{out}^\top\left(e^{\mu}G^\top|\Lambda|PG-|\Lambda|P\right)\xi_{out}\\
&+\frac{e^{\mu}\bar\lambda}{\kappa_1}\xi_{out}^\top\xi_{out}+\ell\theta^\top\theta\\
&+\int_0^1\xi^\top\left(M^\top\mathcal{P}(y)+\mathcal{P}(y)M-\mu|\Lambda|\mathcal{P}(y)\right)\xi dy\\
&+\lambda_{\max}\kappa_2\int_0^1\xi^\top(y,t)\xi(y,t)dy+\frac{\lambda_{\max}}{\kappa_2}|b|^2\\
\leq&-\nu V(t)+\alpha\left(|(b,\theta(t))|^2\right),
\end{aligned}\tag{50}$$

where $\alpha=\max\left(\ell,\frac{\lambda_{\max}}{\kappa_2}\right)$.

From the definition of the candidate ISS-Lyapunov function V in (41), we have, for all $\xi\in L^2\left((0,1),\mathbb{R}^{2N}\right)$

$$\lambda_{max}^{-1}\|\xi\|_{L^2}^2\leq V(\xi)\leq\lambda_{max}\|\xi\|_{L^2}^2. \tag{51}$$

Therefore, according to (50), (51) and Definition 2, V defined by (41) is an ISS-Lyapunov function for the network of traffic flow (30), (34), then the system (30) with (34) is ISS, as stated in the statement of Theorem 1.

This concludes the proof of Theorem 1. ■

TABLE I
TRAFFIC PARAMETERS AND CONTROL GAINS IN THE SIMULATION.

	$j=1$	$j=2$	$j=3$	$j=4$
I_j	4	4	4	4
$L_j\,(km)$	1	1	1	1
k_j^ρ	60	60	60	60
k_j^v	0.4	0.4	0.4	0.4
$\rho_j^*\,(veh/h)$	85	95	105	115
$v_j^*\,(km/h)$	90	80	70	60

Remark 3: As the conditions (39)-(40) of Theorem 1 involve the spatial variable, the number of inequality constraints is infinite. While, the inequalities can be solved by using the polytopic embedding method for $y \in [0, L]$, such as the algorithms proposed in Proposition 1 of [23] or Proposition 4.5 of [12]. ○

IV. SIMULATION AND EXPERIMENT

A. Numerical Simulation

The purpose of this subsection is to verify the design of the ISS boundary stabilization given by the inequality conditions of Theorem 1 through the numerical simulation.

We consider a local freeway network including four links, in which the first two upstream links are in the free-flow regime but the following two downstream links are in the congestion regime, i.e. $M = 2$, $N = 4$. The traffic parameters of roads are given as $v_f = 150km/h$, $\rho_m = 200veh/km$, $a = 0.75$, $\tau = 100s$, and the demand disturbances $|\tilde{p}_{in}(t)| \leq 50\ veh/h$, $|\tilde{s}_j(t)| \leq 50\ veh/h$, for all $j = 1, 2, 3, 4$. The other traffic parameters and control gains specific to each link are shown in Table I.

For the specific network of traffic flow of (30), we have the state variable

$$\xi = \left[\ \tilde{\omega}_1 \quad \dots \quad \tilde{\omega}_4 \quad \tilde{z}_1 \quad \dots \quad \tilde{z}_4\ \right]^\top, \tag{52}$$

the system matrices

$$\Lambda = \text{diag}\{90, 80, 70, 60, 26.25, 8.75, -8.75, -26.25\}, \tag{53}$$

$$M = \begin{bmatrix} M_1 & 0 \\ M_1 & 0 \end{bmatrix}, \tag{54}$$

with $M_1 = \text{diag}\{-0.01, -0.01, -0.01, -0.01\}$, and the model drift

$$b = \left[\ b_1 \quad b_1\ \right]^\top, \tag{55}$$

with $b_1 = \left[\ -0.0375 \quad -0.0125 \quad 0.0125 \quad 0.0375\ \right]^\top$.

For the specific boundary feedback control of (34), the input and output variables are given as

$$\xi_{in} = \left[\ \tilde{\omega}_1(0,t) \quad \tilde{\omega}_2(0,t) \quad \tilde{\omega}_3(0,t) \quad \tilde{\omega}_4(0,t) \quad \tilde{z}_1(0,t) \quad \tilde{z}_2(0,t) \quad \tilde{z}_3(1,t) \quad \tilde{z}_4(1,t)\ \right]^\top, \tag{56}$$

$$\xi_{out} = \left[\ \tilde{\omega}_1(1,t) \quad \tilde{\omega}_2(1,t) \quad \tilde{\omega}_3(1,t) \quad \tilde{\omega}_4(1,t) \quad \tilde{z}_1(1,t) \quad \tilde{z}_2(1,t) \quad \tilde{z}_3(0,t) \quad \tilde{z}_4(0,t)\ \right]^\top, \tag{57}$$

and the boundary condition matrix

$$G = \begin{bmatrix} G_{11} & G_{12} \\ 0 & G_{22} \end{bmatrix}, \tag{58}$$

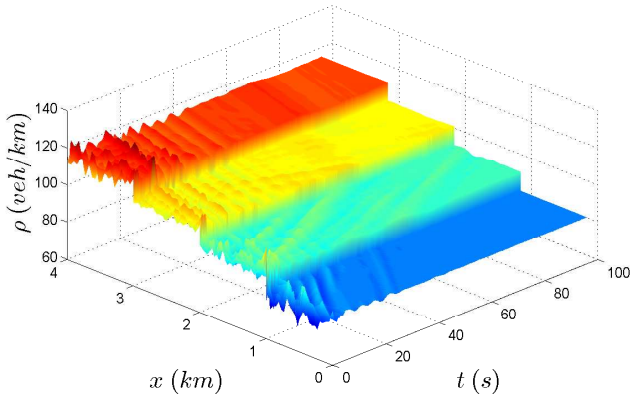

Fig. 5. The time and space evolution of the vehicle density of the freeway traffic under the boundary feedback control (34).

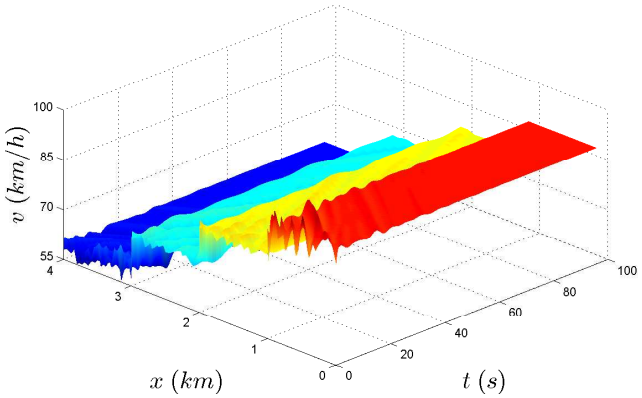

Fig. 6. The time and space evolution of the vehicle speed of the freeway traffic under the boundary feedback control (34).

with

$$G_{11} = \begin{bmatrix} 0.17 & 0 & 0 & 0 \\ 1.13 & 0.19 & 0 & 0 \\ 0 & 1.14 & 0.21 & 0 \\ 0 & 0 & 1.17 & 0.25 \end{bmatrix},$$

$$G_{12} = \begin{bmatrix} -0.05 & 0 & 0 & 0 \\ -0.33 & -0.14 & 0 & 0 \\ 0 & -0.13 & -0.21 & 0 \\ 0 & 0 & 0.06 & -0.54 \end{bmatrix},$$

$$G_{22} = \text{diag}\{0.4, 0.4, 0.4, 0.4\}.$$

The disturbance of the traffic demand $\theta(t)$ in (34) is given as $\theta(t) = [\theta_1(t), \theta_2(t), \theta_3(t), \theta_4(t), 0, 0, 0, 0]^\top$, with $|\theta_1(t)| \leq \frac{5}{48}$, $|\theta_2(t)| \leq \frac{15}{128}$, $|\theta_3(t)| \leq \frac{15}{112}$, and $|\theta_4(t)| \leq \frac{5}{32}$.

Taking $\mu = 0.1$, and solving the inequality conditions (39)-(40) of Theorem 1, we obtain the diagonal matrix

$$P = \text{diag}\{1.1087, 0.5544, 0.2548, 0.0950, 2.1075, 5.3017, 4.9068, 1.6748\}, \tag{59}$$

with scales $\kappa_1 = 18.1686 > 0$, and $\kappa_2 = 0.0116 > 0$.

To numerically compute the traffic flow dynamics of the local freeway network, we discretize the linearized ARZ model (52)-(58) in time and space simultaneously by using a two-step variant of the Lax-Wendroff method [17]. Then the spatial-temporal evolutions of the vehicle density and the speed are

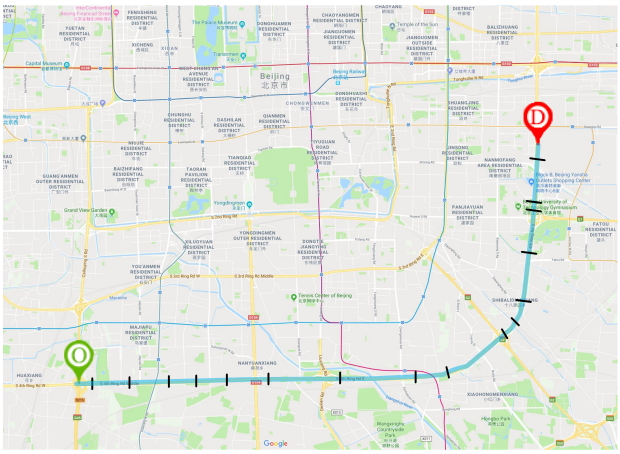

Fig. 7. Google Maps of the research route on Fourth-Ring road of Beijing. The black bars represent the boundaries of the links divided.

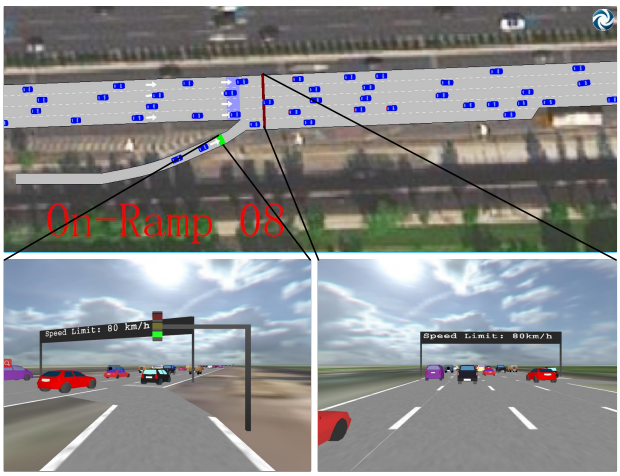

Fig. 8. The 2D and 3D microscopic view of the traffic simulation in the Aimsun software.

shown in Fig. 5 and Fig. 6, respectively. It can be clearly observed that the traffic states ρ_j and v_j, $j = 1, 2, 3, 4$ of each link are converging to the boundedness domains of the desired state (ρ_j^*, v_j^*) ultimately even under the model drift and the unknown demand disturbance.

B. Traffic Experiment with Aimsun

In this subsection, an experiment of freeway traffic control is conducted on the Fourth-Ring road of Beijing, China, based on the traffic simulation software, AIMSUN 6.1 of [2] developed by Transport Simulation Systems.

The Fourth-Ring road is a closed circle freeway in the urban area of Beijing. The selected freeway network is started from MAJIALOU located in the southwest Fourth-Ring road, and ended at DAJIAOTING located in the southeast Fourth-Ring road, with a total length about 17.1km. Its mainline road has four 3.75m wide lanes in each direction. The local freeway network contains sixteen on-ramps and fifteen off-ramps. We define a continuous stretch between the adjacent two on-ramps as a single link despite of the number of off-ramps. Therefore, the studied road can be divided into seventeen links as shown in Fig. 7. Neglecting the upstream road before the first on-ramp, we name the road between the first on-ramp and the second on-ramp link one, and so on.

Using a satellite map including the road as the base map, the local freeway network is embedded in the AIMSUN simulation environment. The traffic detectors and VMSs are placed at the upstream and downstream boundaries of the links to collect the traffic parameters and update the speed limit information in real time. The traffic signal is set up at the entrance of each on-ramp to meter the driving-in vehicles.

AIMSUN can perform dynamic information interaction with the external applications through the AIMSUN application programming interface (API) module while running simulation. In order to implement the boundary feedback control (34) in the simulation, a python script needs to be written to interact with AIMSUN. Through the script, the real-time traffic parameters collected at the road boundaries are directly investigated to calculate the on-ramp metering rate of the traffic lights and the speed limit of VMSs.

In the AIMSUN experiment, to regulate the vehicles that drive into the mainline by means of the traffic light, instead of considering the flow rate $u_j(t)$ as the on-ramp metering control variable, the metering rate $r_j(t) \in [0, 1]$, $j = 1, \ldots, 16$, is adopted. In this case, the on-ramp metering controller is replaced by

$$r_j(t) = \frac{u_j(t)}{u_j^C}, \tag{60}$$

where u_j^C represents the capacity of the on-ramp j.

Once the setting of the freeway network is completed, the traffic demand can be loaded into the AIMSUN OD module according to the statistic data from the Beijing traffic development annual report. The concrete traffic parameters are given as $p_{in}^* = 17000veh/h$, $v_f = 150km/h$, $\rho_m = 200veh/km$, the saturated on-ramp metering rate $u_s = 1600veh/h$. Some traffic parameters of roads and the control gains specific to each link are shown in Table II, in which the feedback gains k_j^ρ, k_j^v, $j = 1, \ldots, 16$, are selected to satisfy the inequality conditions (39)-(40) of Theorem 1.

The total simulation horizon is 60 minutes. The total control period is 30 minutes which is starting from the 31th minute of the simulation (i.e. no control is applied for the first 30 minutes in the simulation), and the control law is updated every minute as same as the traffic signal cycle. The green lights of the on-ramp metering is varying from the minimal 20 seconds to the maximal 60 seconds. The concrete 2D and 3D perspective of the simulation is shown in Fig. 8, respectively.

It should be noted that the traffic data of AIMSUN are the microscopic vehicle trajectories, while the proposed boundary feedback control is based on the macroscopic ARZ traffic flow model. Therefore, we firstly use the kernel density estimation (KDE) of [6], a statistical technique, to aggregate the microscopic vehicle trajectories into the macroscopic density and speed parameters. Suppose the spatial boundaries of a road are a and b, i.e. vehicle position $x \in (a, b)$, let x_i and v_i represent the position and speed of vehicle i, S represents the gross amount of vehicles, then the macroscopic density can

TABLE II
TRAFFIC PARAMETERS AND CONTROL GAINS OF EACH LINK OF THE LOCAL FREEWAY NETWORK.

j	$L_j\,(m)$	I_j	$s_j^*\,(veh/h)$	$u_j^*\,(veh/h)$	$\rho_j^*\,(veh/km)$	$v_j^*\,(km/h)$	k_j^ρ	k_j^v
1	892	4	2000	960	53	80	40	0.3
2	1118	4	1000	1120	59	70	40	0.3
3	698	4	0	970	53	80	40	0.3
4	881	4	0	950	64	70	40	0.3
5	1172	4	1000	1000	72	60	40	0.3
6	1935	4	3000	886	63	65	40	0.3
7	2030	4	1000	899	60	70	40	0.3
8	852	4	1000	1100	54	75	40	0.3
9	1904	4	2000	1161	101	40	60	0.4
10	441	4	0	1098	114	35	60	0.4
11	693	4	0	1308	121	35	60	0.4
12	1130	4	2000	1072	120	35	60	0.4
13	1256	4	1000	990	118	35	60	0.4
14	204	4	0	1131	142	30	60	0.4
15	1035	4	1000	1015	111	40	60	0.4
16	351	4	0	1000	113	40	60	0.4

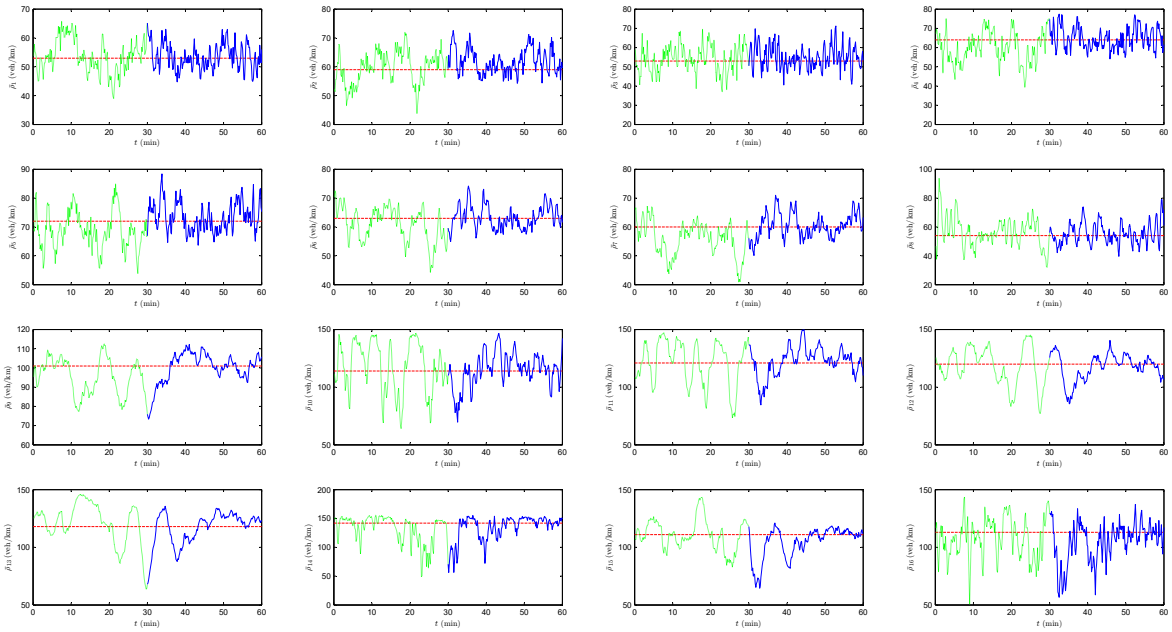

Fig. 9. Time evolution of average density of the freeway network. The dotted green line represents the uncontrolled state, the solid blue line represents the controlled state, and the red dashed line represents the expected steady state.

be computed as

$$\rho(x) = \frac{1}{h}\sum_{i=1}^{S} K\left(x, x_i\right), \tag{61}$$

and the kernel function is taken as

$$\begin{aligned} K\left(x, x_i\right) = \Phi\left(\tfrac{x-x_i}{h}\right) + \Phi\left(\tfrac{x-(2a-x_i)}{h}\right) \\ +\Phi\left(\tfrac{x-(2b-x_i)}{h}\right), \end{aligned} \tag{62}$$

where $\Phi(\cdot)$ represents the standard normal distribution, and the smoothing parameter h chooses 25 meters.

Based on the aggregated average density and speed, we have plotted the time evolutions of ρ_j, v_j of all the sixteen links of the freeway network, as shown in Fig. 9 and 10, respectively. It is can be found that, as we applied the boundary feedback control from the 31th minute, the traffic flow states of all links are ultimately regulated to some boundedness regions.

A comparison of the actual effects for boundary regulation in Fig. 9, 10 indicates that the ultimate ISS bound of the density is larger than one for the speed variable. The main reason is that the actual traffic flux $p_{in}(t)$ set up in AIMSUN has a high fluctuation from the normal flux p_{in}^*, suffering from the influences of stochastic arriving rate, changing line and micro-behavior of traffic. As a result, the vehicular density of the traffic network has a larger ISS bound from the desired state.

C. Discussion

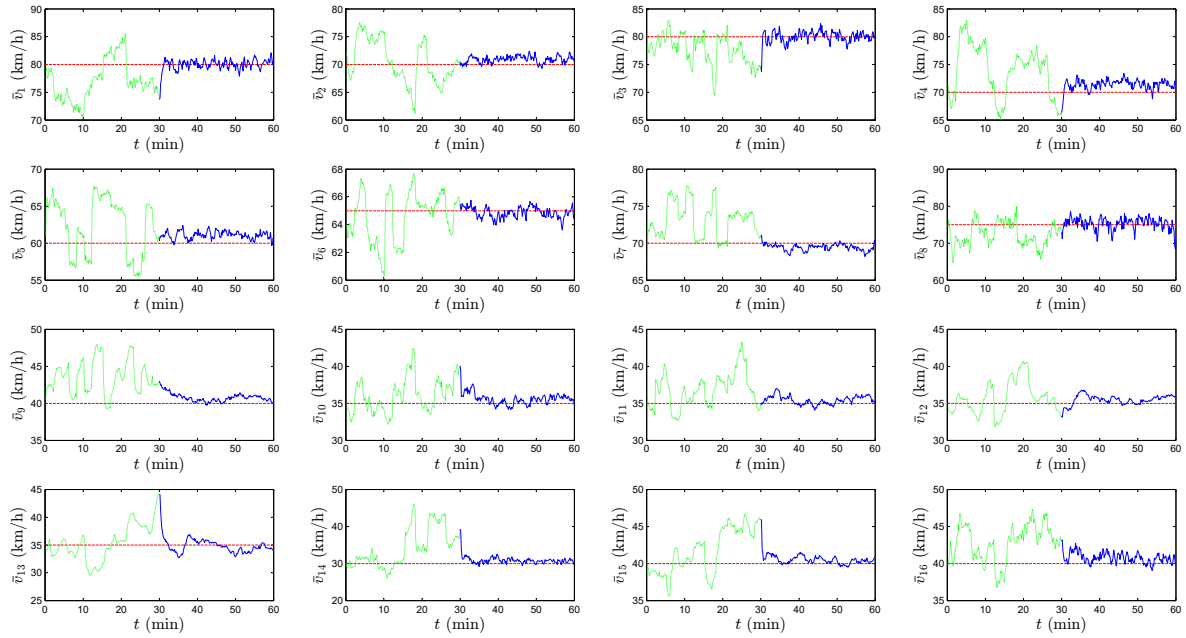

Fig. 10. Time evolution of average speed of the freeway network. The dotted green line represents the uncontrolled state, the solid blue line represents the controlled state, and the red dashed line represents the expected steady state.

From the AIMSUN simulation, we find that the boundary feedback stabilization of freeway traffic is a very interesting and effective aspect for the freeway traffic flow control. Although the total flux rate of each link of the local network is not increasing significantly, the vehicle density and the average speed are regulated to the nearby regions of the desired traffic states. In engineering practice, if all vehicles of the road are traveling with a constant speed, i.e. the consensus traffic state is achieved, the reduced braking behaviours would greatly reduce the vehicle emission, save the fuel and cut down the probability of accidents.

Another interesting finding is the waiting or lost time that vehicles have to queue up at the entrance of the on-ramp for the green light before drives into the mainline. In the simulation, we randomly select 20 vehicles that plan to enter the freeway network from the fourth on-ramp and leave the network from the twelfth off-ramp as the floating cars. All of vehicles' dynamics including the total travel time are recorded and analyzed with the AIMSUN API module. Let us compare the two experimental scenarios: the first group travels during the 30 minutes without control, while the second travels during the following 30 minutes under control. Using the boundary control saves about 12% the average total travel time. The trajectory data show that vehicles have to wait for a period at the on-ramp, generally no more than 100 seconds, while this additional delay is compensated by the shorter travelling time after driving into the mainline of the freeway.

V. Conclusion

In this paper, we address the issue of boundary stabilization for the freeway network of traffic flow which has been modelled with the linearized ARZ equation. Under the disturbance of uncertain demand, a boundary feedback controller which integrates the on-ramp metering and variable speed limit has been designed to regulate the traffic flow staying in the bound region of the desired state. The sufficient condition for the ISS of the network system is given by using the Lyapunov technique. The numerical simulation and the traffic experiment suggest that the proposed boundary control for freeway traffic is feasible and effective.

Future work will target to the reasonable change of traffic modes or desired states according to the traffic data, including and not limited to the traffic demand, road characteristics, and the special circumstance. Another useful extension of this work is to consider the multi-lane traffic dynamics and also the impact of the lane changes.

References

[1] A. Aw and M. Rascle. Resurrection of 'second order' models of traffic flow. *SIAM Journal on Applied Mathematics*, 60(3):916–938, 2000.

[2] J. Barceló and C. Jordi. Dynamic network simulation with AIMSUN. In *Simulation Approaches in Transportation Analysis*, pages 57–98. Springer, 2005.

[3] G. Bastin and J.-M. Coron. *Stability and Boundary Stabilization of 1-D Hyperbolic Systems*. Progress in Nonlinear Differential Equations and Their Applications. Springer, 2016.

[4] N. Bekiaris-Liberis and A.I. Delis. PDE-based feedback control of freeway traffic flow via time-gap manipulation of ACC-equipped vehicles. *IEEE Transactions on Control Systems Technology*, 2020.

[5] C.F. Daganzo. The cell transmission model: A dynamic representation of highway traffic consistent with the hydrodynamic theory. *Transportation Research Part B: Methodological*, 28(4):269–287, 1994.

[6] S. Fan and S. Benjamin. Data-fitted first-order traffic models and their second-order generalizations: Comparison by trajectory and sensor data. *Transportation Research Record*, 2391(2):32–43, 2013.

[7] A. Ferrara, S. Sacone, and S. Siri. *Freeway Traffic Modelling and Control*. Springer, Cham, Switzerland, 2018.
[8] G. Gomes and R. Horowitz. Optimal freeway ramp metering using the asymmetric cell transmission model. *Transportation Research Part C*, 14(2):244–262, 2006.
[9] B. D. Greenshields. A study of traffic capacity. In *Proceedings of the Highway Research Board*, pages 448–477, 1935.
[10] A. Hegyi, B. D. Schutter, and H. Hellendoorn. Model predictive control for optimal coordination of ramp metering and variable speed limits. *Transportation Research Part C*, 13(2):185–209, 2005.
[11] I. Karafyllis, M. Kontorinaki, and M. Papageorgiou. Global exponential stabilization of freeway models. *International Journal of Robust and Nonlinear Control*, (6):1184–1210, 2015.
[12] P.-O. Lamare, A. Girard, and C. Prieur. An optimisation approach for stability analysis and controller synthesis of linear hyperbolic systems. *ESAIM: Control Optim. Calc. Var.*, 22(4):1236–1263, 2016.
[13] M. J. Lighthill and J. B. Whitham. On kinematic waves. II. A theory of traffic flow on long crowded roads. *Proc. R. Soc. A*, pages 317–345, 1955.
[14] A. Mironchenko and C. Prieur. Input-to-state stability of infinite-dimensional systems: recent results and open questions. *SIAM Review*, 62(3):529–614, 2020.
[15] M. Papageorgiou, C. Diakaki, V. Dinopoulou, A. Kotsialos, and Y. Wang. Review of road traffic control strategies. *Proceedings of the IEEE*, 91(12):2043–2067, 2003.
[16] P. I. Richards. Shock waves on the highway. *Oper. Res.*, pages 42–51, 1956.
[17] L.F. Shampine. Two-step Lax–Friedrichs method. *Applied Mathematics Letters*, 18:1134–1136, 2005.
[18] H. Yu and M. Krstic. Traffic congestion control for Aw-Rascle-Zhang model. *Automatica*, 100:38–51, 2018.
[19] H. Yu, L. Zhang, M. Diagne, and M. Krstic. Bilateral boundary control of moving traffic schockwave. *IFAC PapersOnLine*, 52-16:48–53, 2019.
[20] H. M. Zhang. A non-equilibrium traffic model devoid of gas-like behavior. *Transportation Research Part B*, 36(3):275–290, 2002.
[21] L. Zhang and C. Prieur. Necessary and sufficient conditions on the exponential stability of positive hyperbolic systems. *IEEE Transactions on Automatic Control*, 62(7):3610–3617, 2017.
[22] L. Zhang and C. Prieur. Stochastic stability of Markov jump hyperbolic systems with application to traffic flow control. *Automatica*, 86:29–37, 2017.
[23] L. Zhang, C. Prieur, and J. Qiao. Local exponential stabilization of semi-linear hyperbolic systems by means of a boundary feedback control. *IEEE Control Systems Letters*, 2(1):55–60, 2018.
[24] L. Zhang, C. Prieur, and J. Qiao. PI boundary control of linear hyperbolic balance laws with stabilization of ARZ traffic flow models. *Systems & Control Letters*, 123:85–91, 2019.
[25] L. Zhang, C. Prieur, and J. Qiao. Local proportional-integral boundary feedback stabilization for quasilinear hyperbolic systems of balance laws. *SIAM Journal on Control and Optimization*, 58(4):2143–2170, 2020.

Liguo Zhang received the Ph.D. degree in Control Theory and Applications from Beijing University of Technology (BJUT), China, in 2006, and he was a visiting professor (2011-2012) at the Department of Civil and Environmental Engineering, University of California, Berkeley, From 2014, he has been a full professor of the School of Electronic Information and Control Engineering, BJUT.

He is currently the Deputy Director of Faculty of Information Technology, and the Dean of the Department of Artificial Intelligence and Automation, BJUT. His current research interests include hybrid systems, intelligent transportation systems, and control of distributed parameter systems.

He has been an Associate Editor of the *IMA Journal Mathematical Control and Information*, the Guest Editor of the *International Journal of Distributed Sensor Networks*. He was the number of the International Program Committee for the 58th CDC Nice, 2019, and the 59th CDC Jeju Island, 2020.

Haoran Luan received the B.Eng. degree in automation from Shandong Technology and Business University, Yantai, China, in 2018, and he is currently pursuing the Ph.D. degree in control science and engineering from Beijing University of Technology, Beijing, China.

His research interests include intelligent transportation systems and control of distributed parameter systems.

Yusheng Lu received the B.Eng. degree in automation and the M.Sc. degree in control science and engineering from Beijing University of Technology, Beijing, China, in 2017 and 2020.

His research interests include distributed parameter systems and intelligent transportation systems.

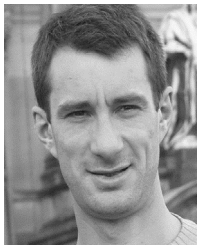

Christophe Prieur received the M.Sc. degree in mathematics from the École Normale Supérieure de Paris-Saclay, Cachan, France, in 2000, and the Ph.D. degree in applied mathematics from Université Paris-Sud, Orsay, France, in 2001.

He has been a Senior Researcher with the French National Centre for Scientific Research, Paris, France, since 2011. His current research interests include nonlinear control theory, hybrid systems, and control of partial differential equations.

He has been a member of European Control Association-Conference Editorial Board (EUCA-CEB), and a member of IEEE-Control Systems Society (CSS) CEB. He was the Program Chair of the 9th IFAC Symposium on Nonlinear Control Systems (NOLCOS 2013) and the 14th European Control Conference (ECC 2015). He has been an associate editor of the *IEEE Trans. on Automatic Control*, the *European J. of Control*, and the *IEEE Trans. on Control Systems Technology*. He is currently an associate editor of the *AIMS Evolution Equations and Control Theory*, and the *SIAM Journal of Control and Optimization*. He is a senior editor of the *IEEE Control Systems Letters*, and an editor of the *IMA J. of Mathematical Control and Information*.

.